https://doi.org/10.5194/tc-2019-186
Preprint. Discussion started: 17 September 2019


The Cryosphere Discussions
Open Access
EGU

# Spatial and temporal variations in glacier surface roughness during melting season, as observed at August-one glacier, Qilian mountains, China

Junfeng Liu[1]*, Rensheng Chen[1], Chuntan Han[1]

[1] Qilian Alpine Ecology and Hydrology Research Station, Key Laboratory of Ecohydrology of Inland River Basin, Northwest Institute of Eco-Environment and Resources, Chinese Academy of Sciences, Lanzhou, China.
*Correspondence to: Junfeng Liu (jfliu121@163.com)*

**Abstract:** The roughness of glacier surfaces is an important factor governing surface albedo and turbulent heat transfer. Previous studies have not directly observed spatial and temporal variation in surface roughness ($z_0$) over a whole glacier and whole melting season. Such observations can do much to help us understand variation in $z_0$ and thus variations in albedo and turbulent heat transfer. This study, at the August-one ice cap in the Qilian mountains, collected three-dimensional ice surface data at plot-scale, using both automatic and manual close-range digital photogrammetry. Data was collected from sampling sites spanning the whole glacier for the whole of the melting season. The automatic site collected daily photogrammetric measurements from July to September of 2018 for a plot near the center of the ice cap; during this time, snow cover gave place to ice and then returned to snow. $Z_0$ was calculated from this data. Manual measurements were taken at sites dotted from terminal to top; they showed that $z_0$ was larger at the snow and ice transition zone than in areas fully snow or ice covered. This zone moved up the ice cap during the melting season. It is clear that persistent snowfall and rainfall both reduce $z_0$. Using data from a meteorological station near the automatic photogrammetry site, we were able to calculate surface energy balances over the course of the melting season. We found that high or rising turbulent heat as a component of surface energy balance tended to produce a smooth ice surface; low or decreasing turbulent heat tended to produce a rougher surface.

**Keywords**: surface roughness, digital photogrammetry, melting season, transition zone, surface energy balance, August-one ice cap

https://doi.org/10.5194/tc-2019-186
Preprint. Discussion started: 17 September 2019


The Cryosphere Discussions

## 1. Introduction

The roughness of ice surfaces is an important control on air-ice heat transfer, on the ice surface albedo, and thus on the surface energy balance(Greuell and Smeets, 2001;Hock and Holmgren, 2005;Irvine-Fynn et al., 2014) The snow and ice surface roughness at centimeter and millimeter scales is also an important parameter in studies of wind transport, snowdrifts, snowfall, snow grain size, and ice surface melt (Bruce and Smeets, 2000;Brock et al., 2006;McClung and Schaerer, 2006;Fassnacht et al., 2009a;Fassnacht et al., 2009b). Radar sensor signals, such as SAR (Oveisgharan and Zebker, 2007), altimeters and scatter meters, are also affected by ice and snow surface roughness (Lacroix et al., 2007;Lacroix et al., 2008). One of the most important of these influences is the aerodynamic roughness of $z_0$, which is related to ice surface topographic roughness in a complex way (Andreas, 2002;Lehning et al., 2002;Smith et al., 2016). Determination of $z_0$ based on topographic roughness is therefore of great interest for energy-balance studies (Greuell and Smeets, 2001).

Glacier surface $z_0$ has been widely but indirectly studied through such methods as eddy covariance (Munro, 1989;Smeets et al., 2000;Smeets and Van den Broeke, 2008), or wind profile (Wendler and Streten, 1969;Greuell and Smeets, 2001;Denby and Snellen, 2002).However, direct measurement of $z_0$ has been shown to be more accurate than previous methods. Micro-topographic measured $z_0$ shows lower scatter than profile measurements over slush and ice (Brock et al., 2006). Current research has increasingly used direct measurement. It has also become clear that it is important to measure $z_0$ over the entire course of the melting season and at many points on the glacier surface, as $z_0$ is prone to large spatial and temporal variation (Brock et al., 2006;Smeets and Van den Broeke, 2008). This variation is due to variations in weather and snowfall (Albert and Hawley, 2002). The direct measurement of $z_0$ allows repeated measurement at many points on the glacier surface, which is not possible with wind profile or eddy covariance methods.

Photogrammetry has been increasingly popular as a method to measure the roughness of snow and ice surfaces roughness. The first use of the technique involved aircraft-mounted cameras on craft flying over snow and ice (Kääb and Vollmer, 2000). Digital photos were taken against a dark background plate. The contrast between the surface photo and the plate could then be quantified as a measure of glacier roughness (Fassnacht et al., 2009a;Fassnacht et al., 2009b;Manninen et al., 2012). A more recent method, as described by Irvine-Fynn et al. (2014), uses modern consumer-grade digital cameras to do close-range photogrammetry at plot scale (small plots of only a few square meters). Appropriate image settings and acquisition geometry allow the collection of high-resolution data (Irvine-Fynn et al., 2014;Smith et al., 2016). Such data allows researchers to investigate roughness with ever greater precision.

Previous researchers have performed some long-term, systematic, direct studies of glacier surfaces (Smeets et al., 1999;Brock et al., 2006;Smeets and Van den Broeke, 2008;Smith et al., 2016). The current study applied such methods to the study of snow and ice surface roughness during melting season at the August-one ice cap. We used both automatic digital photogrammetry and manual photogrammetry. Automatic methods allowed us to monitor daily variations in surface roughness; manual methods allowed us to characterize surface variation along the main glacial flow line. We also recorded meteorological observations, so as to study the impact of weather conditions (e.g. snowfall or rainfall) on surface roughness. This data allowed a further effort to characterize variation of plot-scale $z_0$ from an energy balance perspective.

https://doi.org/10.5194/tc-2019-186
Preprint. Discussion started: 17 September 2019




## 2. Data and methods

### 2.1 Study area and meteorological data

The August-one glacier ice cap is located in the middle of Qilian Mountains on the northeastern edge of the Tibetan Plateau (Figure 1a, 1b). The glacier is a flat-topped ice cap that is approximately 2.3 km long and 2.4 km$^2$ in area. It ranges in elevation from 4550 to 4820m a.s.l. (Guo et al., 2015). This study was conducted during the melting season of 2018, a season characterized by high precipitation.

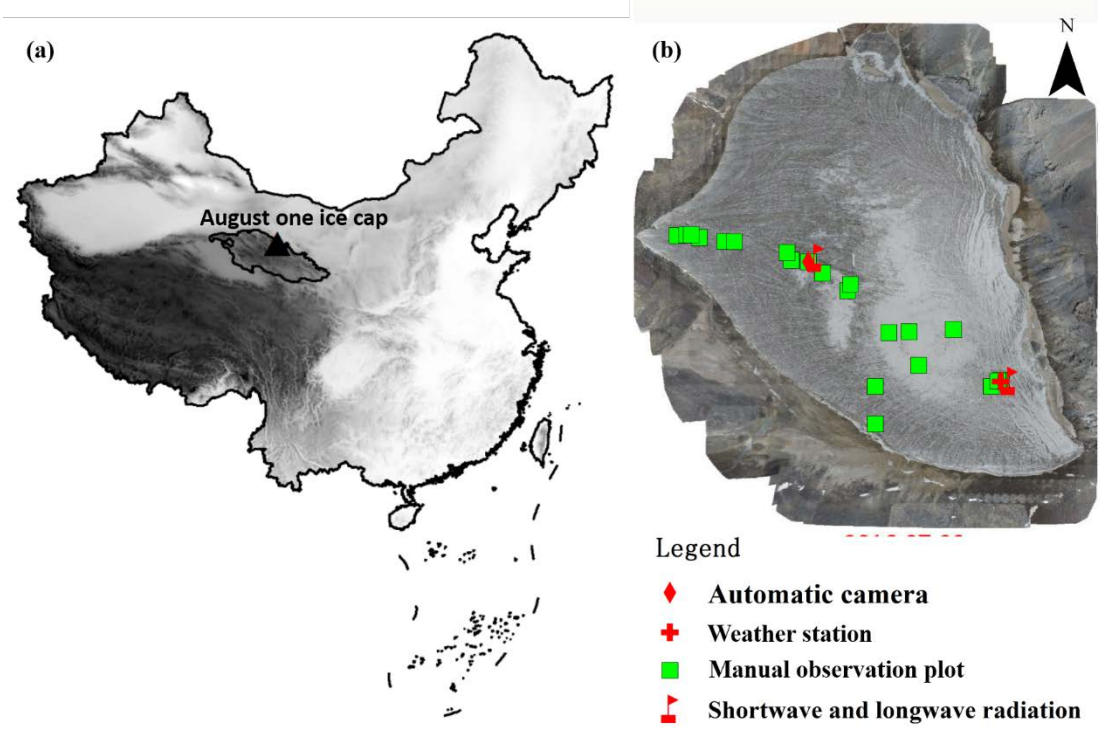


**Figure 1. Location of ice cap and study sites. (a)Location of the August-one glacier, (b)Locations of the AWS, automatic and manual photogrammetry plots, and shortwave observation platforms.**

Researchers had access to meteorological data that had been recorded continuously since September 2015, when an automatic weather station (AWS) was sited at the top of the ice cap. The AWS measures air temperature, relative humidity, and wind speed at 2 and 4 m above the surface. Air pressure, incoming and reflected solar radiation, incoming and outgoing long wave radiation, glacial surface temperature (using an infrared thermometer) are measured at 2 m height. Mass balance is measured by a Campbell Scientific ultrasonic depth gauge (UDG) close to the AWS. An all-weather precipitation gauge with a windbreak fence has been installed about 2 m away from the station. All sensors sample data every 15 seconds. Half-hourly means are stored on a data logger (CR1000, Campbell, USA). Throughout the entire melting season (from June to September) researchers periodically checked the AWS station, to make sure that it remained horizontal and in good

https://doi.org/10.5194/tc-2019-186
Preprint. Discussion started: 17 September 2019


working order. During the entire study period, precipitation total was 261.3mm as measured at the AWS. Of that, 172.1 mm was snow or sleet and 89.2 mm was rainfall (Figure. 7 a).

### 2.2 Automatic photogrammetry

The study began with the placement of an automatic close range photogrammetry measurement apparatus in the middle of the ice cap (4700m (98° 53.4′ E, 39° 1.1′ N. See Figure 1b and Figure2a). It was placed near the existing meteorological station. This was done on July 10, 2018. A wooden frame, 1.5 m wide, and 2 m long, was put on the ice surface. This frame served as a geo-reference control field (Figure. 2b). Four feature points demarcated the control field; three additional points served as check points. A Canon EOS 1300D cameras with an image size of 5184×3456 pixels was connected to the frame. The camera lens was set in wide-angle mode (focal length of 27mm). The f-stop was fixed at f 25 with an exposure time of 1/320s. The camera was programmed to automatically take seven pictures over a period of ten minutes. The photography was repeated at three-hour intervals from 9:00 AM to 18:00 AM, Beijing time. During the ten-minute photography periods, the camera moved along a 1.5 m long slider rail. The seven pictures taken during this period were merged to produce a picture of ice surface topography at millimeter scale (Figure 2b). This apparatus took pictures over a period of three months (July 12 to September 15, the melting season). Sixty-three days of data were recorded. Each daily photography series produced four sets of pictures (twelve hours, three hour intervals). The best-exposed photo sets were used as that day's data. We also set up instrumentation to record incoming and reflected solar radiation. Samples were taken every 15 seconds; 10-minute means were stored on a data logger (CR800, Campbell, USA) located at a height of 1.5m. Mass balance was measured by digital infrared hunting-video camera, which took pictures of ice-surface gauge stakes located near the automatic photogrammetry site.

### 2.3 Manual photogrammetry

Manual close-range photogrammetry was used to survey glacier surfaces at several different locations of the ice cap. Observations were made on four days: July 12 and 25, and later on August 3 and 28. It should be noted that when the July measurements were performed, the ice cap surface was partially snow-covered.

Channels account for only a small portion of the glacier surface area. These surfaces show extreme variability of $z_0$ (Rippin et al., 2015;Smith et al., 2016). For that reason, we distributed the manual photogrammetry study sites over the glacier surface in such a way as to cover most surface types and topographic regions without including any channels [Figure 1b). We photographed a total of thirty-six sites over the four days of observation.

Study plots were demarcated with a 1.1×1.1m portable square aluminum frame. Geo-reference of the point cloud was enabled using control points established by eight cross-shaped screws on the aluminum frame (Figure.2c). Photo pairs (convergent photographs, low oblique photos in which camera axes converge toward one another) were taken at ~1.6 m distances, covering an area of ~1.75 $m^2$. Seven such pairs were taken at each survey site. The camera used was an EOS 6D 50mm, with fixed focal lens and an image size of 5472×3648 pixels. The f-stop was fixed at f 22 with an exposure time from 1/25 to 1/125 s.

https://doi.org/10.5194/tc-2019-186
Preprint. Discussion started: 17 September 2019


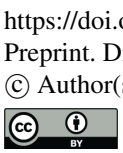



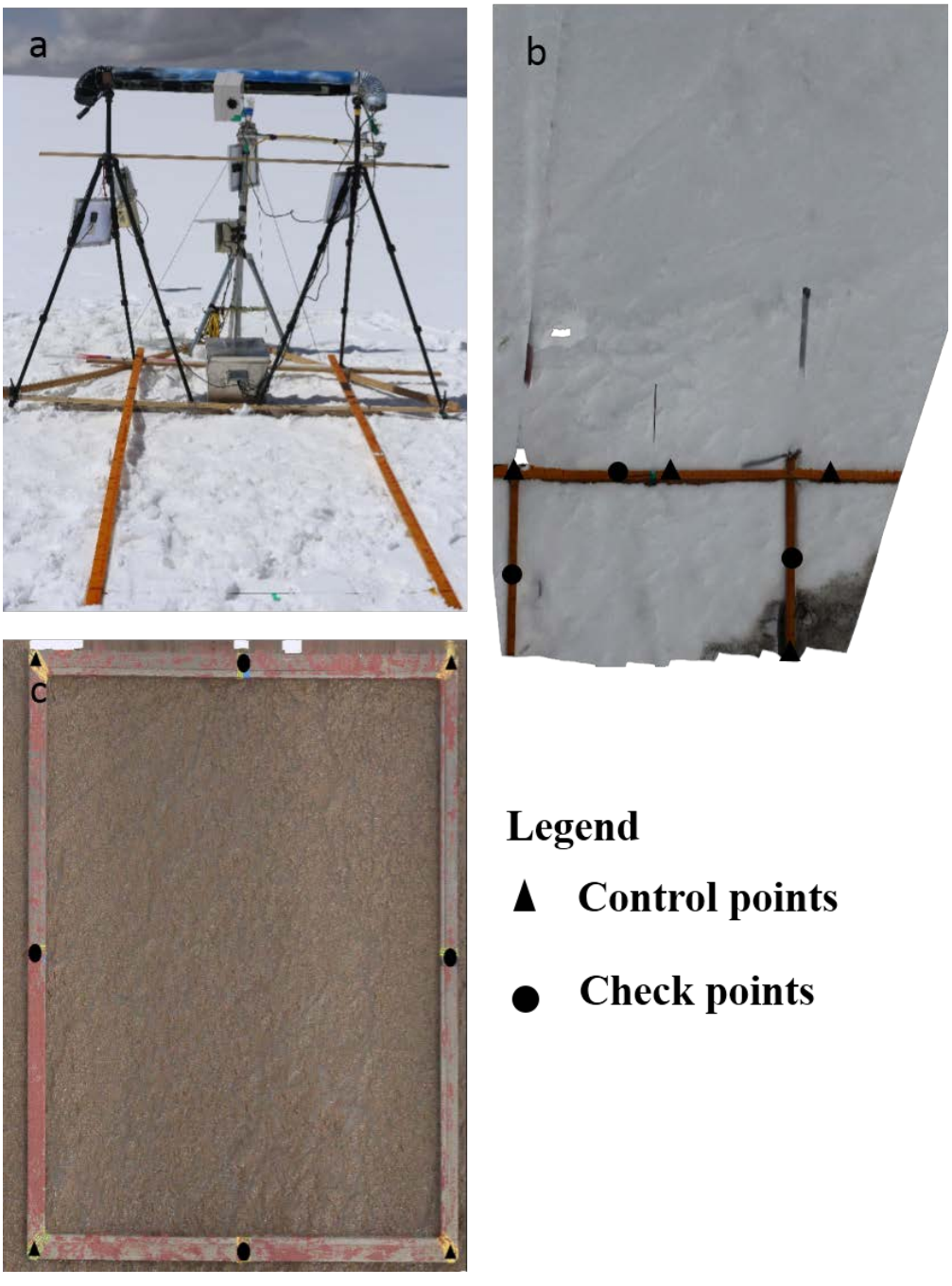


**Figure 2. Frames used for automatic and manual photogrammetry. (a) The automatic photogrammetry device applied in the observation of ice surface roughness in the August-one ice cap. (b) Aluminum frame in situ; ice surface was covered with cryoconite. Four control points and three check points are shown on frame. (c) Manual observation**

https://doi.org/10.5194/tc-2019-186
Preprint. Discussion started: 17 September 2019


**plot; dense point cloud viewed from above; ice surface was covered with cryoconite. Four control points and four check points shown on wooden frame.**

## 2.4 Data processing

Both manual and automatic photographs were imported into a software program, Agisoft Photoscan Professional 1.4.0. This software allowed us to estimate camera intrinsic parameters, camera positions, and scene geometry. Agisoft Photoscan Professional is a commercial package which implements all stages of photogrammetric processing. It has previously been used to generate three-dimensional point clouds and digital elevation models of ice surfaces and braided meltwater rivers (Javernick et al., 2014;Smith et al., 2016).

After new snowfall, it was difficult to match feature points in the photo sets. Three days of automatic data could not be processed. We estimated $z_0$ data for the missing days based on data from snowfall days at the automatic site.

## 2.5 Roughness calculation

Methods for measuring roughness at plot-scale were first developed by soil scientists (Dong et al., 1992;Smith, 2014). Metrics such as the random roughness (RR) or root mean square height deviation (σ), the sum of the absolute slopes (ΣS), the microrelief index (MI), and the peak frequency (the number of elevation peaks per unit transect length) were used. Later these roughness indices were used to describe snow or ice surface roughness (Rees and Arnold, 2006;Fassnacht et al., 2009b;Irvine-Fynn et al., 2014).

Current photogrammetry methods produce high-resolution three-dimensional topographic data. Earlier two-dimensional profile-based methods for estimating surface roughness discard much of the potentially useful three-dimensional topographic data (Passalacqua et al., 2015)(Passalacqua et al. 2015). Smith et al.(2016) were able to use equation (1), developed by Lettau (1969), to make better use of the topographic data, using multiple point clouds and digital elevation models (DEM).

In this method, $z_0$ is quantified as:

$$z_0 = 0.5h^* \frac{s}{S} \qquad (1)$$

where:

$h^*$ represents the effective obstacle height (m) and is calculated as the average vertical extent of micro-topographic variations;

$s$ is the silhouette area facing upwind ($m^2$);

$S$ is the unit ground area occupied by micro-topographic obstacles ($m^2$);

and 0.5 is an averaged drag coefficient.

https://doi.org/10.5194/tc-2019-186
Preprint. Discussion started: 17 September 2019


A profile-based roughness measure can be calculated based on a simplified Lettau equation (see 1 above) by assuming that h* can equal twice the standard deviation of elevations in the de-trended profile, with the profile's mean elevation set to 0 meter. The aerodynamic roughness length for a given profile then becomes

$$z_i = \frac{f}{X}(\sigma_i)^2 \qquad (2)$$

where
*f* is the number of up-crossings above the mean elevation in profile *i*;
X is the length (m) of profile *I*;
and σ is the standard derivation of elevations of profile *i*.

Smith et al. (2016) found that there was little difference between the DEM-based $z_0$ values and values calculated from profiles if the results were averaged over all cardinal wind directions. In this study, we used a DEM-based average $z_0$ of four cardinal wind directions to represent overall surface roughness.

**2.6 Snow and ice surface energy balance calculation**

The temporal variation of $z_0$ at the automatic site was studied from energy balance perspective. The surface heat balance of a melting glacier is given by:

$$Q_M = Q_{is} - Q_{os} + Q_L + Q_E + Q_H + Q_P \qquad (3)$$

where
$Q_M$ is the heat flux of melting;
$Q_{is}$ is the incoming shortwave radiation;
$Q_{os}$ is the outgoing shortwave radiation;
$Q_L$ is the net longwave radiation;
$Q_E$ is the latent heat flux; $Q_H$ is the sensible heat flux;
and $Q_P$ is the heat from rain.

$Q_E$ and $Q_H$ were calculated using a bulk aerodynamic approach, as described in Oke (1987). The heat from rain is given by Konya and Matsumoto (2010):

$$Q_P = \rho_W C_W T_W P_r \qquad (4)$$

where

https://doi.org/10.5194/tc-2019-186
Preprint. Discussion started: 17 September 2019




$\rho_w$ is the density of water(1000 kg $m^{-3}$);
$C_W$ is the specific heat of water (4187.6 J $kg^{-1}$ $K^{-1}$);
$T_W$ is the wet-bulb temperature(K);
and $P_r$ is the rainfall intensity (mm).

In order to calculate $P_r$, we used the air temperatures recorded at the AWS. There is an elevation difference between the study site (4700 m) and the AWS (4790m); recorded air temperatures were corrected to account for the elevation difference, assuming a lapse rate of -7 ℃ $Km^{-1}$. Wind speed and relative humidity at the study sites were assumed to be equal to those observed at the AWS, as measurements taken by the AWS are broadly representative of the whole ice cap.

## 3. Results

### 3.1 Photogrammetry precision

We used seventeen control points and check points to analyze the horizontal and vertical accuracy of our automatic photogrammetry, and thirty-one pairs for our manual photogrammetry. Automatic photogrammetry: average point density of the final plot point clouds was >1,000,000 points $m^{-2}$. DEMs of 0.1mm resolution were generated at plot scale. The average geo-reference errors were less than 1 millimeter (see Tables 1 and 2). Total RMSE of the automatic control points was 3.0 mm, for check points 3.62mm. Vertical error for control points was 3.58mm, and 4.83mm for check points (Tables 1 and 2). Control and check point errors are all within 1 cm. Manual measurements: average point density of the final plot point clouds was >6,000,000 points $m^{-2}$. DEM of 0.1 mm resolution was generated at plot scale. Root mean square error (RMSE) of 4 control points is 1.78 mm (Table 1). Control points vertical accuracy of manual photogrammetry is about 1.65 mm. Total RMSE of manual photogrammetry check points is 0.99 mm, vertical accuracy is 0.66mm (see Tables 1 and 2).

**Table 1 Control point RMSE for manual and automatic photogrammetry**

| | Ground control points | X error (mm) | Y error (mm) | Z error (mm) | Total error (mm) |
|---|---|---|---|---|---|
| Automatic | Point 1 | 0.71 | 5.83 | 6.61 | 5.11 |
| | Point 2 | 0.41 | 1.14 | 0.74 | 0.82 |
| | Point 3 | 0.54 | 4.55 | 2.40 | 2.99 |
| | Point 4 | 0.45 | 0.76 | 1.04 | 0.79 |
| | **Average** | **0.54** | **3.76** | **3.58** | **3.01** |
| Manual | Point 2 | 0.62 | 0.43 | 0.81 | 1.11 |
| | Point 4 | 0.44 | 0.27 | 0.43 | 0.67 |
| | Point 5 | 0.18 | 0.47 | 0.85 | 0.99 |
| | Point 7 | 0.66 | 0.39 | 2.97 | 3.07 |
| | **Average** | **0.52** | **0.40** | **1.65** | **1.78** |

https://doi.org/10.5194/tc-2019-186
Preprint. Discussion started: 17 September 2019




**Table 2 Check point RMSE for manual and automatic photogrammetry**

| | Ground Check points | X error (mm) | Y error (mm) | Z error (mm) | Total error (mm) |
|---|---|---|---|---|---|
| Automatic | Point 5 | 2.06 | 4.44 | 7.70 | 5.27 |
| | Point 6 | 0.91 | 3.56 | 1.95 | 2.40 |
| | Point 7 | 0.98 | 3.11 | 2.60 | 2.41 |
| | **Average** | **1.41** | **3.74** | **4.83** | **3.62** |
| Manual | Point 1 | 0.30 | 0.19 | 0.39 | 0.52 |
| | Point 3 | 0.79 | 0.37 | 0.69 | 1.12 |
| | Point 6 | 0.28 | 0.83 | 0.90 | 1.26 |
| | Point8 | 0.46 | 0.45 | 0.44 | 0.77 |
| | **Average** | **0.52** | **0.53** | **0.66** | **0.99** |

Note that the control and check point errors are larger for the automatic measurements than for the manual ones. We believe that this is the case because, rather than using static f-stop and exposure times (as in automatic photogrammetry) researchers engaged in manual photogrammetry could adjust exposure time based on ice surface conditions. This allowed production of better quality photos even on cloudy or foggy days. (See Figures 3 and 4). However, even automatic measurements satisfied the requirement outlined by Rees and Arnold (2006) that millimeter vertical accuracy was required and would suffice to calculate surface roughness ($z_0$).

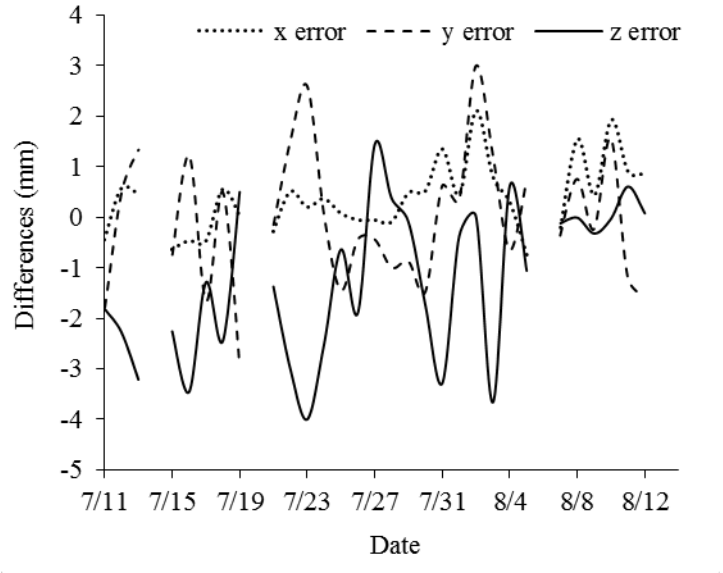


**Figure 3. Automatic photogrammetry checkpoint errors**

https://doi.org/10.5194/tc-2019-186
Preprint. Discussion started: 17 September 2019




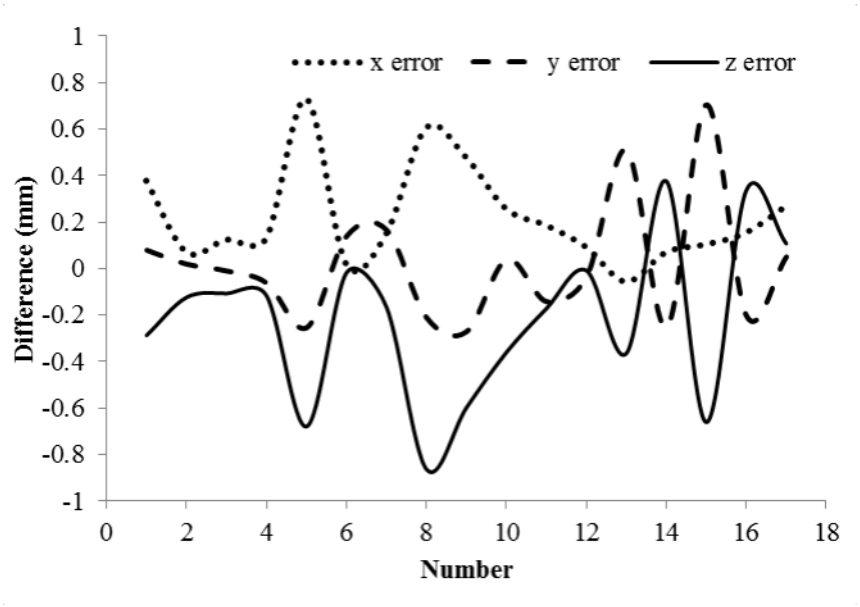


**Figure 4. Manual photogrammetry checkpoint errors**

### 3.2 Surface roughness as measured by automatic photogrammetry

Data for ice surface roughness was collected by the automatic photogrammetry camera site from July 12 to September 15, a period covered the whole melting season. Profile and DEM data show that $z_0$ was highly variable over the study period (Figure 5). The profile data shows a $z_0$ varying from 0.05 mm to 2.74mm (mean: 0.45 mm). The DEM data shows a $z_0$ varying from 0.02mm to 2.56 mm (mean: 0.51 mm).

- At the start of the observation period snow covered the study site.
- As the snow melted, glacier surface $z_0$ increased (save during periods of intermittent snowfall, when $z_0$ dropped to ~0.1mm).
- On July 21, cryoconite appeared on patches of snow-crust, which led to patchy melt.
- From July 21 to 24, overall $z_0$ increased from 0.1mm to 1.6mm.
- By July 29, snow had disappeared from the study site; $z_0$ fluctuated but trended lower.
- From July 29 to August 5 bare ice covered whole field of view; $z_0$ ranged from 0.18 to 0.56mm.
- From August 6 to September 3 there was intermittent snowfall followed by melting; $z_0$ ranged from 0.1 to 1.0mm.
- From September 4 to September 14 $z_0$ showed an overall increase, reaching a maximum of 2.5 mm on September 8. There was intermittent snowfall during this period, which temporarily reduced $z_0$. $Z_0$ then increased thanks to patchy micro-scale melting.
- After September 14, snow covered the whole surface of the glacier. There was no melting and little fluctuation in $z_0$.

https://doi.org/10.5194/tc-2019-186
Preprint. Discussion started: 17 September 2019




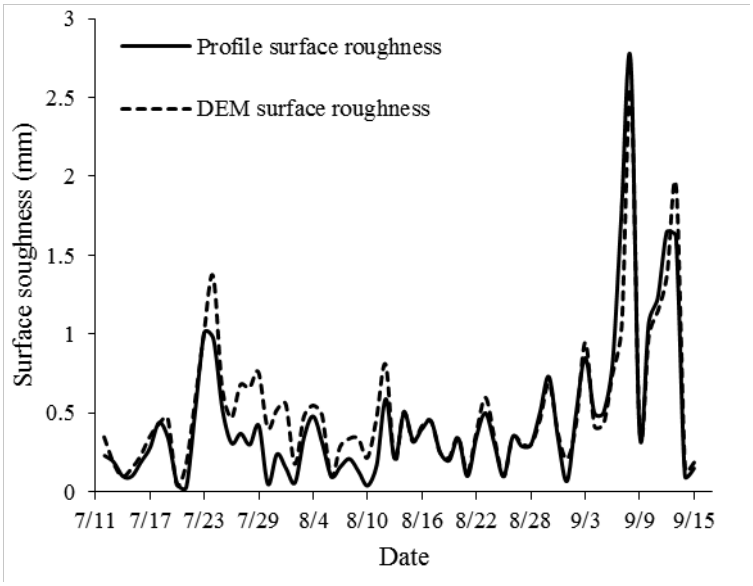


**Figure 5. Variation of ice surface roughness over time, automatic observation site**

It should be clear that $z_0$ varied greatly during melting season. There were two peaks in $z_0$, both of which occurred in period of transition: snow surface turning to ice around July 24 and ice surface turning to snow on September 8. On July 24 and again on September 8 and 13, glacier surfaces featured cryoconite holes and snow crust. Both the automatic and manual observations showed the same pattern: maximum $z_0$ at snow-ice transition belt during partially snow-covered periods.

### 3.3 Surface roughness as measured by manual photogrammetry

Ice surface roughness proved to have an interesting relation with altitude and date. $Z_0$ was highest in the transition zone between snow cover and ice. This zone moved up the ice cap during the melting season.

On July 12, ice surface roughness decreased from 3.2mm to 0.25mm as altitude increased (Figure. 6a, r= 0.8429, P=0.0006<0.01). Near the ice cap terminal of 4590m, the ice surface featured porous snow/ice and many cryoconite holes. As altitude increased, the number of cryoconite holes decreased and snow coverage increased. At 4700m the ice surface was predominantly snow covered, and only a few small patches were bare of snow.

On July 25, ice surface roughness fluctuated between 0.27 to 0.65 mm at the ice cap terminal (4593m). At ~4700m, roughness increased to 1.85mm. Above that point, roughness gradually decreased to 0.25mm at the ice cap top, which was covered by snow (Figure 6b).

On August 3, the August-one ice cap was predominantly bare ice; there was scattered snow crust at the ice cap top. The ice surface, (terminal to top) showed a heavy deposit of cryoconite (Figure 1c). Manual investigation revealed that ice surface roughness increased with altitude (Figure. 6c, r=0.7, P=0.01<0.05). From terminal to top, $z_0$ varied from 0.06 mm to 2.2 mm.

On August 29, the ice cap surface roughness showed no significant correlation with altitude (Figure. 6d, r=-0.03, P=0.9>0.5). $Z_0$ varied from 0.2 mm to 0.98 mm (Figure6 d).

https://doi.org/10.5194/tc-2019-186
Preprint. Discussion started: 17 September 2019




When we compare the results of the four surveys, we see that ice surface roughness was quite variable. Maximum $z_0$ was seen at the snow and ice transition zone, where the ice surface featured both cryoconite holes and clean snow crust. Snow crust would have inhibited melting; cryoconite would have increased it. It is thus understandable that surface roughness would have been greater in such an area. Bare ice or snow cover both result in comparatively less roughness.

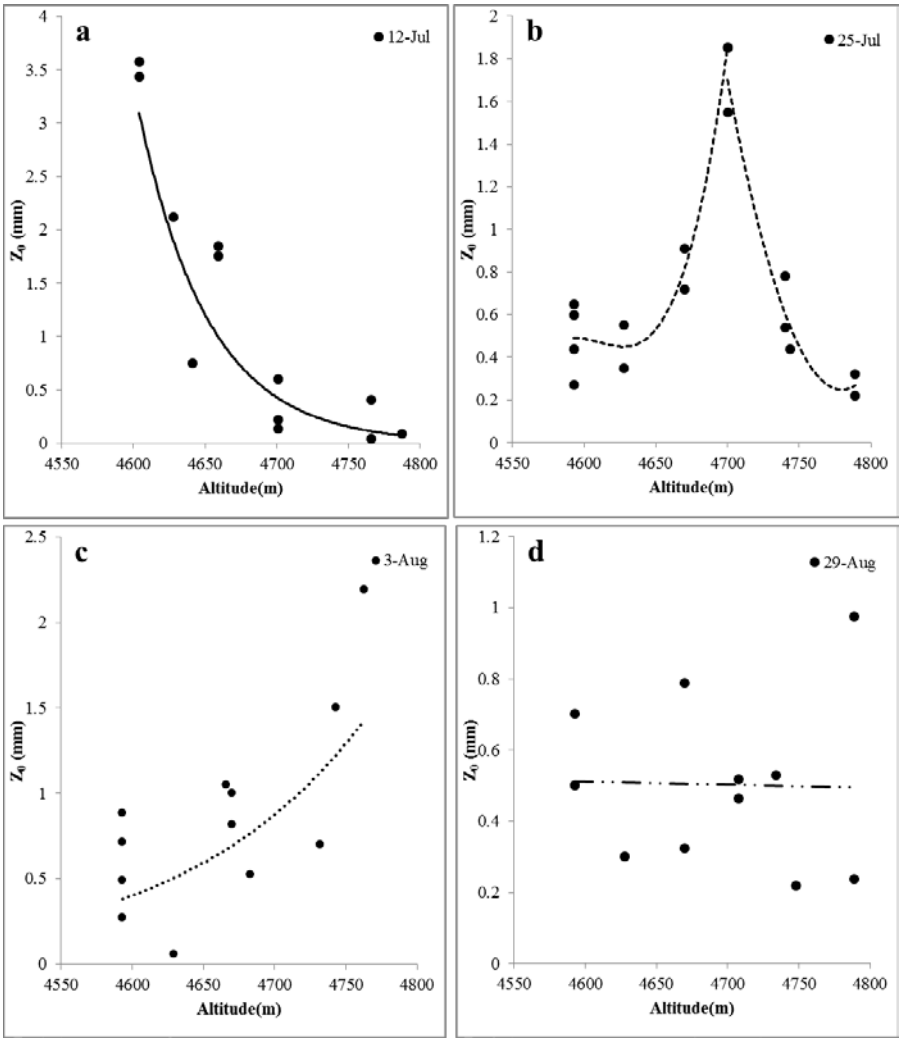


**Figure 6. Surface roughness vs. altitude, (a) As observed on 12 July, (b) As observed on 25 July, (c) As observed on 3 August, (d) As observed on 28 August.**

### 3.4 $Z_0$ and weather

Snowfall was recorded from July 12 to 24. In general, snowfall reduced roughness if it resulted in a fully snow-covered surface. However, if a patchy, shallow snow cover was formed, it tended to increase $z_0$ after a short drop. For example, on August 11 and 12, two successive sleety days created a patchy snow cover which soon increased $z_0$. Between July 26 and August 31 there were sixteen rainfall events, which tended to lower ice surface $z_0$.

https://doi.org/10.5194/tc-2019-186
Preprint. Discussion started: 17 September 2019


Daily temperatures during the study period ranged from -6.5 °C to 7.1 °C (mean: 1.3, Figure. 7b). It was 1.2 °C on July 11. It increased to 3.6 °C on July 24 (the date when $z_0$ was highest). It continued increasing until July 29, when it reached its highest annual of 7.1 °C. During this period $z_0$ continuously declined. From July 28 to end of August temperatures fluctuated between -0.3 to 5.7 °C with no evident trend. $Z_0$ also fluctuated slightly, showing no obvious trend. In September air temperature quickly dropped from 0.6 to -6.5 °C. There were large fluctuations in $z_0$ during this period. The largest fluctuations appeared when air temperatures dropped from positive to negative.

Daily mean solar radiation fluctuated dramatically during the study period due to cloud and overcast (Figure. 7c). Incident solar radiation fluctuated between 129W $m^{-2}$ and 753 W $m^{-2}$ (mean: 469 W $m^{-2}$). From July 29 to end of August, the weather was cloudy, warm, calm, and humid most of the time (Figure. 7b, 7d 7e), and $z_0$ was relatively stable except when there was intermittent snowfall-induced fluctuation. After in September, the weather was again becoming cold and dry and $z_0$ was quite variable.

### 3.5 Ice-surface energy balance at automatic $z_0$ observation study site

Glacier surface melt and roughness are mainly governed by net shortwave and longwave radiation, sensible heat, and latent heat. The following section analyzes the changes in surface energy balance at the automatic site. Our records allowed us to study the factors that control ice surface roughness.

#### 3.5.1 Net radiation

Net radiation varied from -9.7 to 260.2 W $m^{-2}$ (mean: 95.3 W $m^{-2}$) during the study period. This constituted the largest energy flux affecting glacier-surface energy balance. It accounted for 84% of total incoming flux (Figure. 8). Net radiation was relatively low in the first thirteen days of the study period (mean: 69.3 $Wm^{-2}$), when the glacier surface was covered with snow. In the succeeding five days, net radiation increased to 103.9 W $m^{-2}$. At this time the ice surface exhibited a patchwork of snow, ice, and cryoconite.

From July 29 to August 5 the surface of the study site was composed of ice with a dusting of cryoconite. Net radiation reached a height of 183 $Wm^{-2}$. There was intermittent snowfall from August 6 to September 8. Net radiation dropped to a mean 93 $Wm^{-2}$. Snow cover then appeared and net radiation dropped to a low of 46 $Wm^{-2}$.

https://doi.org/10.5194/tc-2019-186
Preprint. Discussion started: 17 September 2019




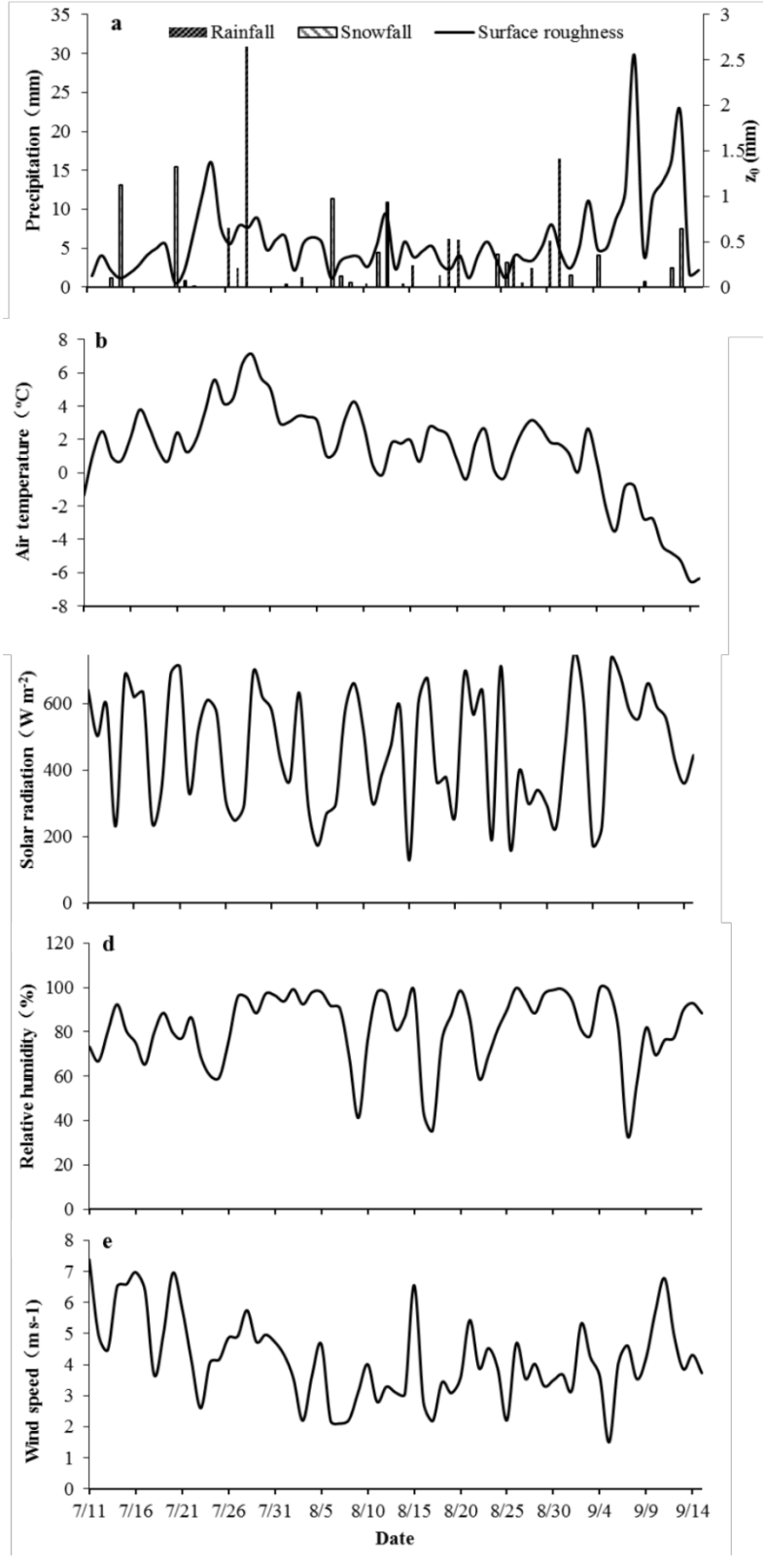




320

https://doi.org/10.5194/tc-2019-186
Preprint. Discussion started: 17 September 2019




**Figure 7. Weather conditions at AWS over study period. (a) Precipitation, (b) Air temperature, (c) Incident solar radiation, (d) Relative humidity, (e) Wind speed.**

### 3.5.2 Sensible heat

Sensible heat ($Q_H$) was the second largest energy-flux component of in surface energy balance during the study period (Figure 7). The sensible heat daily mean varied from -7.1 to 66.3 W m$^{-2}$. It accounted for -28% to 32% (mean: 15%) of the net energy flux.

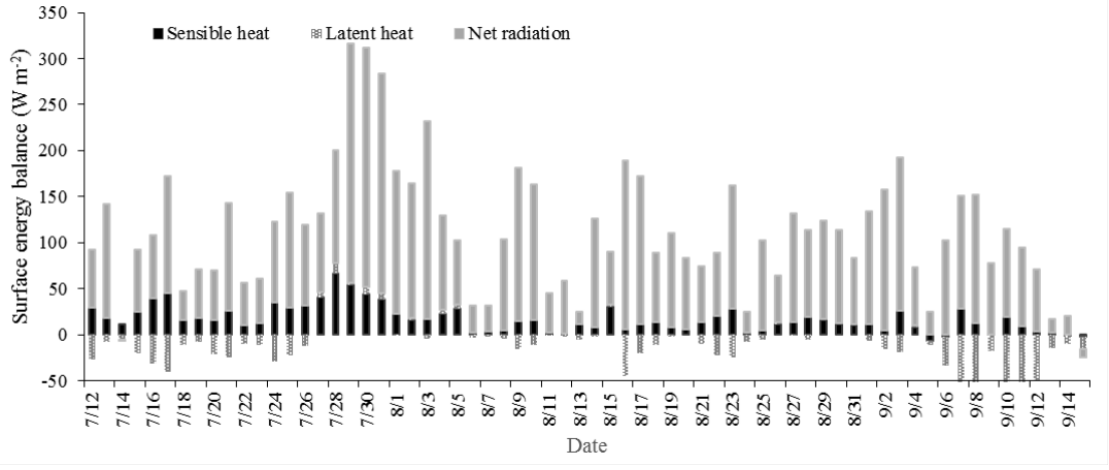


**Figure 8 Daily mean of energy balance at the middle of glacier study site close to the automatic photogrammetry site.**

### 3.5.3 Latent heat

Latent heat was generally small throughout the study period. Daily mean of latent heat varied from -80.1 to 11.1 W m$^{-2}$ (mean: -13.2 W m$^{-2}$). It account for a mere 0.9% for the total incoming flux. It was negative from July 11 to 26 when the ice surface was snow covered. After July 26 the latent heat was mainly positive in the following ten days (ice surface was pure ice or partially snow covered). From August 6 to the end of the study period (September 15) it was predominantly negative.

### 3.5.4 Energy from rainfall

From July 25 to August 5 rainfall energy varied from 0 to 11.7 W m$^{-2}$ (mean: 0.3W m$^{-2}$). Rainfall accounted for a mere 0.2% of total incoming flux. One event accounted for much of the total: on July 28 a 31mm rainfall event added a flux of 11.7 W m$^{-2}$, which resulted in visible smoothing of the ice surface (Figure 8).

### 3.5.5 Surface ablation modeled versus observed

https://doi.org/10.5194/tc-2019-186
Preprint. Discussion started: 17 September 2019




Based on the previously listed measurements of energy fluxes we calculated the probable surface ablation at the automatic photogrammetry site. We took into account observed net radiation, calculated turbulent heat fluxes, and heat from rainfall. There was good agreement between the model and observed results (Figure 9). This suggests that our calculation of turbulent heat based on observed $z_0$, as entered in the model, matches the observed ablation. Such indirect observations could be useful in modeling the ablation process at other glacier study sites. We also found that the modeled mass balance did not match measurement results obtained on days with mixed snow and rain. It is likely that $z_0$ was more than usually variable at those times. Measurements on a finer temporal scale might be needed for calculation of turbulent heat fluxes.

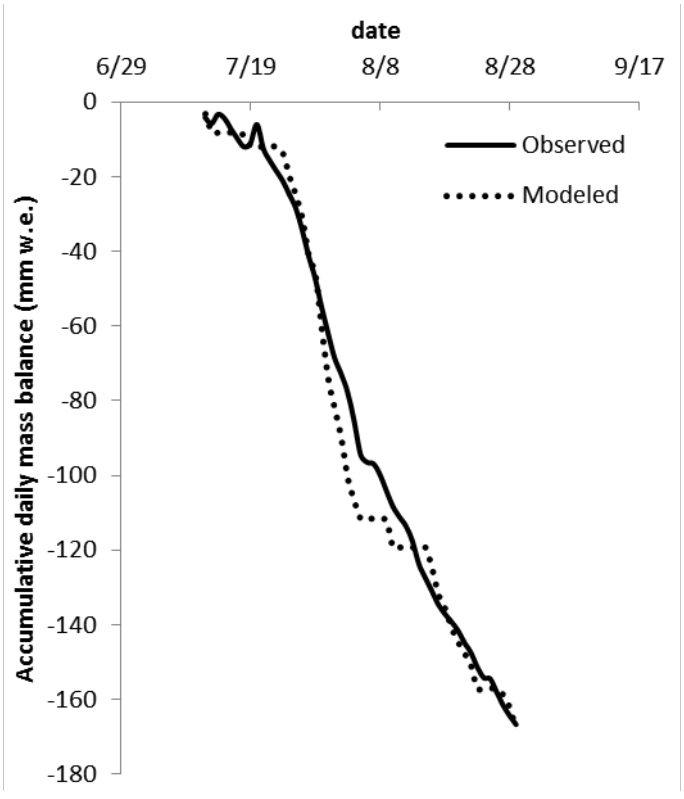


**Figure 9. Comparison of daily mass balance observed and daily mass balance as modeled. Mass balance measurements were taken from 12 July to August 29. Measurements of surface lowering were converted into water equivalents using density values.**

Figure 10 shows the relationship between observed $z_0$ and the main energy flows. These scatter diagrams showed no significant relationship between $z_0$ and net shortwave radiation, longwave radiation, and sensible heat (Figure 10a, 10b, 10c). Graphing $z_0$ vs. latent heat showed a significant negative exponential relationship (Figure 9d, r= -0.61, P=0.0001<0.001). When latent heat is higher, as it is during the melting seas, $z_0$ decreases.

https://doi.org/10.5194/tc-2019-186
Preprint. Discussion started: 17 September 2019




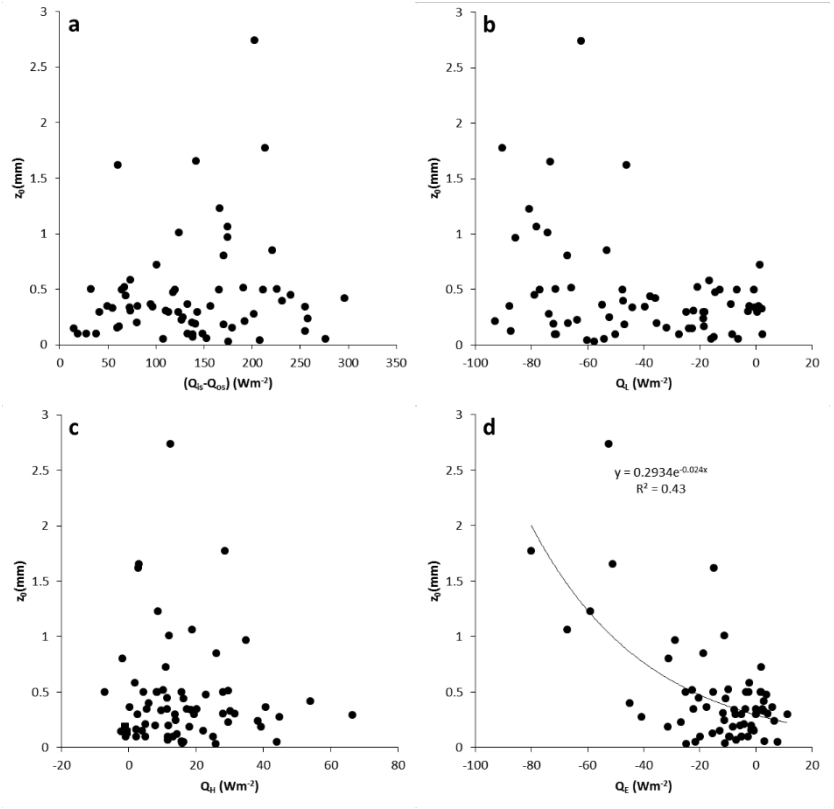


**Figure 10. Surface roughness vs. energy inputs. (a) Surface roughness vs. net shortwave radiation, (b) Surface roughness vs. net longwave radiation, (c) Surface roughness vs. sensible heat, (d) Surface roughness vs. latent heat.**

Because net shortwave radiation and turbulent heat fluxes were the main energy fluxes affecting ice surface roughness, we calculated a turbulent heat proportion index:

$$L_S=(Q_H+Q_E+Q_P)/(Q_{is}-Q_{os}) \quad (5)$$

We then graphed $z_0$ vs. $L_S$ (see Figure 11). A strong exponential relationship was evident (Figure 11a, r= -0.45, P=0.002<0.005). Note that $z_0$ on days when snow fell was strongly affected by the amount of the snowfall. If we exclude snowfall days, we see an even more significant exponential relationship between $z_0$ and $L_S$ (Figure 11b, r= -0.62, P=0.0001<0.001)).

The $z_0$ vs. $L_S$ graph indicates that when turbulent and rainfall heat increased, roughness decreased. In other words, a sunny and cold day facilitates rough ice surfaces; warm and cloudy days tend to produce a smoother ice surface. When net shortwave radiation is higher, and if latent and sensible heat were higher, $z_0$ tends to be smaller; if latent and sensible heat were smaller, $z_0$ would tend to be higher. When net shortwave radiation is smaller, as on cloudy days, any snowfall or rainfall is usually associated with smaller $z_0$. Under a negative $Q_M$, the surface $z_0$ would be not affected by melting process.

https://doi.org/10.5194/tc-2019-186
Preprint. Discussion started: 17 September 2019


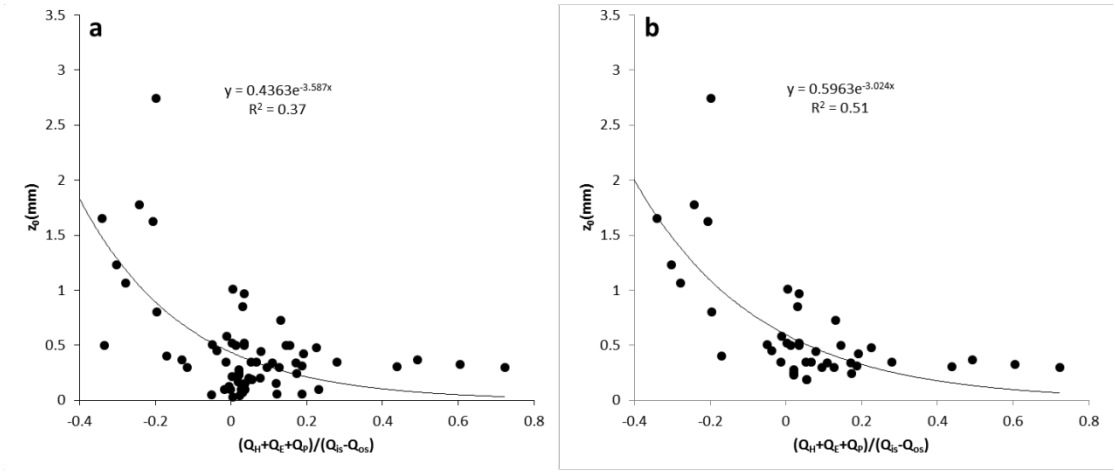


**Figure 11. Surface roughness vs. $L_S$. Where $L_S=(Q_H+Q_E+Q_P)/(Q_{is}-Q_{os})$, (a) Including snowfall days, (b) Excluding snowfall days.**

## 4. Discussion

### 4.1 Automatic and manual photogrammetric methods

Photogrammetric techniques such as Structure from Motion (SfM) (James and Robson, 2012) and Multi-view Stereo (MVS) represent a low-cost option for acquiring high-resolution topographic data. Such approaches require relatively little training and are extremely inexpensive (Fonstad et al., 2013;Passalacqua et al., 2015).

We used both automatic and manual photogrammetric methods to sample spatial and temporal $z_0$ variation at the August-one ice cap. One interesting finding: manual photogrammetry is more precise than automatic photogrammetry (Tables 1 and 2). However, precision is not always the major concern. The glacier surface was a harsh, even punishing environment for the researchers doing manual photogrammetry. In addition, manual photogrammetry took much longer. Automatic methods reduced hours of field work, spared researchers, and produced nearly continuous data. Cloudy or frosty weather affected automatic photogrammetry exposures, and heavy snowfalls resulted in a texture-less surface. Nevertheless, it is likely that photogrammetry techniques will continue to improve and that these drawbacks may be mitigated.

### 4.2 Spatial and temporal variability of $z_0$

Previous studies of glacier surfaces roughness rarely have covered the whole glacier, from terminal to top, in one melting season (Föhn, 1973;Smeets et al., 1999;Denby and Smeets, 2000;Greuell and Smeets, 2001;Albert and Hawley, 2002;Brock et al., 2006;Smeets and Van den Broeke, 2008;Smith et al., 2016). Our study may have been the first to do so.

https://doi.org/10.5194/tc-2019-186
Preprint. Discussion started: 17 September 2019


Whole-glacier study allowed us to follow the movement of the transition zone, where snow was melting and exposing ice, from terminal to top. The transition zone moved up as the melting season proceeded, so roughening the surface of the glacier and raising $z_0$.

At the start of the melting season, snow cover first disappeared, leaving an ice surface, at the terminal end of the glacier, that is, at the lower altitude. This newly exposed surface was rougher ($z_0$ was higher) than on the upper part of glacier, which was still snow covered (see the black line Figure 6a for $z_0$ distribution at different altitudes). As the snowline shifted to higher altitudes, ice surface increased, as did $z_0$ (see the dashed black curve in Figure 6b). As the melting continued, the snow and ice transition belt reached the top of glacier (see the dotted curve in Figure 6c). When the glacier was completely free of snow, $z_0$ and elevation were no longer correlated (see the dotted-dashed line in Figure 6d).

In sum: maximum $z_0$ was recorded at the cross-glacier transition zone between snow and ice. This zone shifted from lower altitude to higher altitude, from terminal to top, during the melting season.

Micro-topography (Föhn, 1973;Smeets et al., 1999;Irvine-Fynn et al., 2014), wind profile, and eddy covariance methods generate a wide range of $z_0$ values for snow and ice surfaces (Brock et al., 2006). It should be noted that *averaged* values for $z_0$ matched those found in other studies. $Z_0$ for *snow-covered* surfaces ranged from 0.01 to 3.5mm (mean: 0.5mm). These results match values reported in other studies, which ranged from 0.1 to 8.2 mm (Munro, 1989;Hock and Holmgren, 2005;Schneider, 1999;Grainger and Lister, 1966).

$Z_0$ for *ice surfaces* ranged from 0.01 to 2.5mm (mean: 0.6). Our results also match values reported in studies reporting results ranging from. 0.1mm to 6.9mm (Brock et al., 2006;Guo et al., 2018;Sun et al., 2018). Our results showed that $z_0$ reached its maximum at the end of the summer melt, which matched indirect measurements by Smeets and Broeke (2008).

Previous studies have shown that freshly fallen snow is subject to rapid destructive metamorphism (McClung and Schaerer, 2006), which can dramatically change the roughness of fresh snow surfaces (Fassnacht et al., 2009b). Our study showed that $z_0$ could be quite variable during melting season. Intermittent snowfall first decreased snow surface $z_0$, which then began to increase as the snow surface deteriorated. With the appearance of cryoconite, $z_0$ rose to its greatest value.

### 4.3 Effects of surface energy balance components on surface roughness

Aerodynamic roughness is associated with the geometry of ice roughness elements (Kuipers, 1957;Lettau, 1969;Munro, 1989). Surface geometry roughness develops due to local melt inhomogeneities in melting season. In this study, our results show that $L_s$ (turbulent heat index; see Section 3.5.5, equation 5) is a determining factor in directly measured $z_0$. A high index was associated with a smooth ice surface; a low or even a negative index was associated with rough surfaces. Hence at the end of melting season, ice surfaces would be at their very roughest when $L_s$ reached to its lowest.

The August-one ice cap is a heavy-loading glacier; cryoconites are unevenly distributed over the ice surface. On clear days shortwave radiation caused heterogeneous melt: cryoconite-covered ice quickly melted and formed rough ice surfaces. Under cloudy or rainy days, turbulent heat is dominant, and ice surface roughness decreased. This process resembles the process by which cryoconite holes develop and decay. In that process, cryoconite holes develop when the radiative flux is dominant and decay when turbulent heat is dominant (McIntyre, 1984;Takeuchi et al., 2018).

https://doi.org/10.5194/tc-2019-186
Preprint. Discussion started: 17 September 2019


This study found an exponential relationship between $z_0$ and $L_s$. These results suggest that quantitative rather than qualitative research will be of great help to researchers hoping to understand ice surface roughness.

## 5. Conclusions

Manual and automatic measurements of snow and ice surface roughness at the August-one ice cap showed great spatial and temporal variation in $z_0$ over the melting season. Manual measurements, taken from terminal to glacier top, show that the nature of the surface cover features are correlated with $z_0$ rank in this order: transition region > pure ice area or pure snow area. The transition region forms a zone of maximum $z_0$, which shifts, over the melting season, from terminal to top. The observed $z_0$ vs energy items analysis indicated that $L_S$ (turbulent heat index) was also an important determinant of ice surface roughness.

Surface roughness is a major parameter in calculations of glacier-surface turbulent heat fluxes. In previous studies investigators used a constant $z_0$ value for the whole surface of the glacier. This study captures much smaller scale variation spatial and temporal glacier surface aerodynamic roughness through automatic and manual photogrammetric observations. Such close observation of variation in $z_0$ certainly enhanced the accuracy of the surface energy balance models developed in the course of this study.

Of course, this study covered only one glacier. It is not clear that it is typical of other Qilian glaciers, or of glaciers in the rest of the world. Further studies are necessary.

## Acknowledgements

This study was supported by the National Natural Sciences Foundation of China (41877163, 41671029).

https://doi.org/10.5194/tc-2019-186
Preprint. Discussion started: 17 September 2019


**References**

Albert, M. R., and Hawley, R. L.: Seasonal changes in snow surface roughness characteristics at Summit, Greenland: implications for snow and firn ventilation, Annals of Glaciology, 35, 510-514, 10.3189/172756402781816591, 2002.

Andreas, E. L.: Parameterizing scalar transfer over snow and ice: A review, Journal of Hydrometeorology, 3, 417-432, 2002.

Brock, B. W., Willis, I. C., and Sharp, M. J.: Measurement and parameterization of aerodynamic roughness length variations at Haut Glacier d'Arolla, Switzerland, Journal of Glaciology, 52, 1-17, 2006.

Bruce, D., and Smeets, C. J. P. P.: Derivation of turbulent flux profiles and roughness lengths from katabatic flow dynamics, Journal of applied Meteorology, 39, 12, 2000.

Denby, B., and Smeets, C.: Derivation of turbulent flux profiles and roughness lengths from katabatic flow dynamics, Journal of applied Meteorology, 39, 1601-1612, 2000.

Denby, B., and Snellen, H.: A comparison of surface renewal theory with the observed roughness length for temperature on a melting glacier surface, Boundary-layer meteorology, 103, 459-468, 2002.

Dong, W. P., Sullivan, P. J., and Stout, K. J.: Comprehensive study of parameters for characterizing three-dimensional surface topography I: Some inherent properties of parameter variation, Wear, 159, 161-171, 1992.

Föhn, P. M. B.: Short-term snow melt and ablation derived from heat-and mass-balance measurements, Journal of Glaciology, 12, 275-289, 1973.

Fassnacht, S. R., Stednick, J. D., Deems, J. S., and Corrao, M. V.: Metrics for assessing snow surface roughness from digital imagery, Water Resources Research, 45, W00D31, 10.1029/2008wr006986, 2009a.

Fassnacht, S. R., Williams, M., and Corrao, M.: Changes in the surface roughness of snow from millimetre to metre scales, Ecological Complexity, 6, 221-229, 10.1016/j.ecocom.2009.05.003, 2009b.

Fonstad, M. A., Dietrich, J. T., Courville, B. C., Jensen, J. L., and Carbonneau, P. E.: Topographic structure from motion: a new development in photogrammetric measurement, Earth Surface Processes and Landforms, 38, 421-430, 10.1002/esp.3366, 2013.

Grainger, M., and Lister, H.: Wind speed, stability and eddy viscosity over melting ice surfaces, Journal of Glaciology, 6, 1966.

Greuell, W., and Smeets, P.: Variations with elevation in the surface energy balance on the Pasterze (Austria), Journal of Geophysical Research: Atmospheres, 106, 31717-31727, 2001.

Guo, S. h., Chen, R. s., Liu, G. h., Han, C. t., Song, Y. x., Liu, J. f., Yang, Y., Liu, Z. w., Wang, X. q., and Liu, X. j.: Simple Parameterization of Aerodynamic Roughness Lengths and the Turbulent Heat Fluxes at the Top of Midlatitude August‐One Glacier, Qilian Mountains, China, Journal of Geophysical Research: Atmospheres, 123, 12,066-012,080, 10.1029/2018JD028875, 2018.

Guo, W., Liu, S., Xu, J., Wu, L., Shangguan, D., Yao, X., Wei, J., Bao, W., Yu, P., Liu, Q., and Jiang, Z.: The second Chinese glacier inventory: data, methods and results. Journal of Glaciology, Journal of Glaciology, 61, 10.3189/2015jog14j209, 2015.

Hock, R., and Holmgren, B.: A distributed surface energy-balance model for complex topography and its application to Storglaciären, Sweden, Journal of Glaciology, 51, 25-36, 10.3189/172756505781829566, 2005.

Irvine-Fynn, T., Sanz-Ablanedo, E., Rutter, N., Smith, M., and Chandler, J.: Measuring glacier surface roughness using plot-scale, close-range digital photogrammetry, Journal of Glaciology, 60, 957-969, 10.3189/2014JoG14J032, 2014.

https://doi.org/10.5194/tc-2019-186
Preprint. Discussion started: 17 September 2019


James, M., and Robson, S.: Straightforward reconstruction of 3D surfaces and topography with a camera: Accuracy and geoscience application, Journal of Geophysical Research: Earth Surface, 117, F03017, 10.1029/2011JF002289, 2012, 2012.

Javernick, L., Brasington, J., and Caruso, B.: Modeling the topography of shallow braided rivers using Structure-from-Motion photogrammetry, Geomorphology, 213, 166-182, 10.1016/j.geomorph.2014.10.006, 2014.

Kääb, A., and Vollmer, M.: Surface geometry, thickness changes and flow fields on permafrost streams: automatic extraction by digital image analysis, Permafrost and Periglacial Processes, 11, 10.1002/1099-1530(200012)11:4<315::AID-PPP365>3.0.CO;2-J, 2000.

Konya, K., and Matsumoto, T.: Influence of weather conditions and spatial variability on glacier surface melt in Chilean Patagonia, Theoretical and applied climatology, 102, 139-149, 2010.

Kuipers, H.: A relief meter for soil cultivation studies, Netherlands Journal of Agricultural Science, 5, 255-262, 1957.

Lacroix, P., Legrésy, B., Coleman, R., Dechambre, M., and Rémy, F.: Dual-frequency altimeter signal from Envisat on the Amery ice-shelf, Remote Sensing of Environment, 109, 285-294, 10.1016/j.rse.2007.01.007, 2007.

Lacroix, P., Legrésy, B., Langley, K., Hamran, S., Kohler, J., Roques, S., Rémy, F., and Dechambre, M.: In situ measurements of snow surface roughness using a laser profiler, Journal of Glaciology, 54, 753-762, 10.3189/002214308786570863, 2008.

Lehning, M., Bartelt, P., Brown, B., and Fierz, C.: A physical SNOWPACK model for the Swiss avalanche warning: Part III: meteorological forcing, thin layer formation and evaluation, Cold Regions Science and Technology, 35, 10.1016/S0165-232X(02)00072-1, 2002.

Lettau, H.: Note on aerodynamic roughness parameter estimation the basis of roughness element description, Journal of Applied Meteorology, 8, 1969.

Manninen, T., Anttila, K., Karjalainen, T., and Lahtinen, P.: Automatic snow surface roughness estimation using digital photos, Journal of Glaciology, 58, 993-1007, 10.3189/2012JoG11J144, 2012.

McClung, D., and Schaerer, P. A.: The avalanche handbook, The Mountaineers Books, Seattle, WA, 2006.

McIntyre, N. F.: Cryoconite hole thermodynamics, Canadian Journal of Earth Sciences, 21, 1984.

Munro, D. S.: Surface roughness and bulk heat transfer on a glacier: comparison with eddy correlation, Journal of Glaciology, 35, 343-348, 10.3189/S0022143000009266, 1989.

Oke, T. R.: Boundary layer climates, Routledge, London, 1987.

Oveisgharan, S., and Zebker, H. A.: Estimating snow accumulation from InSAR correlation observations, IEEE Transactions on Geoscience and Remote Sensing, 45, 10-20, 10.1109/TGRS.2006.886196, 2007.

Passalacqua, P., Belmont, P., Staley, D. M., Simley, J. D., Arrowsmith, J. R., Bode, C. A., Crosby, C., DeLong, S. B., Glenn, N. F., Kelly, S. A., Lague, D., Sangireddy, H., Schaffrath, K., Tarboton, D., Wasklewicz, T., and Wheaton, J. M.: Analyzing high resolution topography for advancing the understanding of mass and energy transfer through landscapes: A review, Earth-Science Reviews, 148, 174-193, 10.1016/j.earscirev.2015.05.012, 2015.

Rees, W. G., and Arnold, N. S.: Scale-dependent roughness of a glacier surface: implications for radar backscatter and aerodynamic roughness modelling, Journal of Glaciology, 52, 214-222, 10.3189/172756506781828665, 2006.


Rippin, D. M., Pomfret, A., and King, N.: High resolution mapping of supra - glacial drainage pathways reveals link between micro - channel drainage density, surface roughness and surface reflectance, Earth Surface Processes and Landforms, 40, 1279-1290, 10.1002/esp.3719, 2015.

Schneider, C.: Energy balance estimates during the summer season of glaciers of the Antarctic Peninsula Global Planetary Change, 22, 10.1016/S0921-8181(99)00030-2, 1999.

Smeets, C., Duynkerke, P., and Vugts, H.: Observed wind profiles and turbulence fluxes over an ice surface with changing surface roughness, Boundary-Layer Meteorology, 92, 101-121, 1999.

Smeets, C. J. P. P., Duynkerke, P. G., and Vugts, H. F.: Turbulence characteristics of the stable boundary layer over a mid-latitude glacier. Part II: Pure katabatic forcing conditions, Boundary-layer meteorology, 97, 73-107, 2000.

Smeets, C. J. P. P., and Van den Broeke, M. R.: Temporal and spatial variations of the aerodynamic roughness length in the ablation zone of the Greenland ice sheet, Boundary-layer meteorology, 128, 315-338, https://doi.org/10.1007/s10546-008-9291-0, 2008.

Smith, M. W.: Roughness in the earth sciences, Earth-Science Reviews, 136, 202-225, 2014.

Smith, M. W., Quincey, D. J., Dixon, T., Bingham, R. G., Carrivick, J. L., Irvine - Fynn, T. D. L., and Rippin, D. M.: Aerodynamic roughness of glacial ice surfaces derived from high - resolution topographic data, Journal of Geophysical Research: Earth Surface, 121, 748-766, 10.1002/2015JF003759, 2016.

Sun, W. j., Qin, X., Wang, Y. t., Chen, J. z., Du, W. t., Zhang, T., and Huai, B. j.: The response of surface mass and energy balance of a continental glacier to climate variability, western Qilian Mountains, China, Climate dynamics, 50, 3557-3570, 10.1007/s00382-017-3823-6, 2018.

Takeuchi, N., Sakaki, R., Uetake, J., Nagatsuka, N., Shimada, R., Niwano, M., and Aoki, T.: Temporal variations of cryoconite holes and cryoconite coverage on the ablation ice surface of Qaanaaq Glacier in northwest Greenland, Annals of Glaciology, 59, doi: 10.1017/aog.2018.19, 2018.

Wendler, G., and Streten, N.: A short term heat balance study on a coast range glacier, pure and applied geophysics, 77, 68-77, 1969.